Tilt transitions in compressively strained AgTa_{0.5}Nb_{0.5}O_{3} thin films

R. L. Johnson-Wilke, D. S. Tinberg, C. B. Yeager, Y. Han, I. M. Reaney, I. Levin, D. D. Fong, T. T. Fister, and S. Trolier-McKinstry

Phys. Rev. B **84**, 134114 — Published 24 October 2011

DOI: 10.1103/PhysRevB.84.134114

Tilt transitions in compressively strained $AgTa_{½}Nb_{½}O_3$ thin films

R. L. Johnson-Wilke[1], D. S. Tinberg[1], C.B. Yeager[1], Y. Han[2], I. M. Reaney[3], I. Levin[4], D. D. Fong[5], T. T. Fister[6], and S. Trolier-McKinstry[1]

[1] Materials Research Institute and Materials Science and Engineering Department, Pennsylvania State University, University Park, PA 16802, USA
[2] Nanoscale Physics Research Laboratory, School of Physics and Astronomy, University of Birmingham, Birmingham B15 2TT, UK
[3] Department of Engineering Materials, University of Sheffield, Sir Robert Hadfield Building, Mappin Street, Sheffield S1 3JD, United Kingdom
[4] Ceramics Division, National Institute of Standards and Technology, Gaithersburg, MD 20899, USA
[5] Materials Science Division, Argonne National Laboratory, Argonne, IL 60439, USA
[6] Chemical Sciences and Engineering Division, Argonne National Laboratory, Argonne, IL 60439, USA

Abstract

Phase transitions in coherently strained epitaxial $AgTa_{½}Nb_{½}O_3$ films grown on $SrTiO_3$ (001) substrates were characterized by high resolution X-ray diffraction and transmission electron microscopy. Coherently strained films were found to undergo the same phase transition sequence as bulk materials: cubic (C) ↔ tetragonal (T) ↔ orthorhombic (O) ↔ orthorhombic (M_3). However, the compressive in-plane strain stabilized the tetragonal and orthorhombic phases, expanding these phase fields by ≈ 280 °C. The compressive strain state also favors *c*-axis domain texture. Consequently, unit cell quadrupling in the M_3 phase and the in-phase tilt of the T phase both occur around the out-of-plane direction. In contrast, bulk materials and relaxed films are poly-domain, with the complex tilt system occurring along all three of the orthogonal axes. Compressively strained films are in the M_3 phase at room temperature rather than in the M_2 phase as is observed in bulk. This suggests that strain not only modifies octahedral rotations but also disrupts the ordering of local cation displacements. These results demonstrate unambiguously that strain engineering in systems with *complex* tilt sequences such as $AgTa_{½}Nb_{½}O_3$ is feasible and open up the possibility of modifying properties by manipulation of the pertinent octahedral tilt transition temperature in a wide range of functional ceramics.

Introduction

In many materials with the ABO_3 perovskite crystal structure, the corner-linked [BO_6] octahedral framework undergoes cooperative rotations accompanied by the onset of spontaneous strain. In bulk materials, such transitions have a profound impact on piezoelectric coefficients, on relative permittivity and on the temperature coefficient of resonant frequency in microwave dielectrics.[1-3] However, relatively little work has been reported on the link between octahedral tilt and strain in films. Density functional theory predicts that in-plane strains influence rotations of the oxygen octahedra.[4-6] These calculations suggest that biaxial compressive strain enhances the tilt angle of the octahedral rotations about the out-of-plane axis. Conversely, for materials under tensile biaxial strain, tilting around in-plane axes is favored. He *et al*.[7,8] reported that both compressive and tensile in-plane strains enhanced the tilt transition

temperature of $SrTiO_3$. May *et al*., in their study of $LaNiO_3$ films, quantified octahedral tilt and B-O-B bond angles by comparing measured and calculated intensities of superlattice reflections.[9] Biaxial compressive strain led to larger tilt angles about the out-of-plane axis whereas biaxial tensile strain favored in-plane tilt. Similar results were found in $La_{0.67}Sr_{0.33}MnO_3$ and $SrRuO_3$ films grown on a variety of substrates that induced different levels of strain.[10] In superlattice structures that consisted of $LaNiO_3$ (tilted) and $SrMnO_3$ (untilted) layers, a decrease in tilt angle and bond length was observed as the thickness of the tilted layer decreased.[11] In other reports, strain was used to modify the room temperature phase as well as phase transition temperatures in tilted systems such as $SrRuO_3$ and $CaRuO_3$ thin films.[12-14] The materials choice in these published works deals with systems that exhibit relatively simple tilt structures. The research presented in this manuscript examines a more complicated perovskite material, $AgTa_xNb_{1-x}O_3$, which undergoes a complex behavior of octahedral rotations that is in turn coupled to local cation displacements.

$AgTa_xNb_{1-x}O_3$ (ATN) has been studied in recent years as temperature stable ceramics for high frequency capacitors.[15-18] Moreover, density functional theory calculations predict that $AgNbO_3$ is a useful end member in PbO-free solid solutions for piezoelectric applications.[19] ATN solid solutions exhibit a complex sequence of tilting phase transitions.[20-22] For ceramics x=0.5, the phase transition sequence, space groups and Glazer tilt systems are listed in Table 1 in which all phases except cubic exhibit tilted octahedra.

Table 1 Space group and tilt system for the material $AgTa_{½}Nb_{½}O_3$.[20,21,23]

Phase	Space Group	Tilt System	Transition Temperature
Cubic (C)	*Pm3m*	$a^0a^0a^0$	*C↔T: 552 °C*
Tetragonal (T)	*P4/mbm*	$a^0b^0c^+$	*T↔O: 400 °C*
Orthorhombic (O)	*Cmcm or Pbcn*	$a^0b^-c^+$	*O↔M₃: 326 °C*
M_3, M_2, and M_1	*Pbcm*	$a^-b^-c^-/a^-b^-c^+$	*M₃↔M₂: 46 °C* *M₂↔M₃: -13 °C*

The M phases all have the same space group and tilt system, $a^-b^-c^-/a^-b^-c^+$, (Figure 1) with anti-phase tilting about the *a*- and *b*- axes, and a periodic sequence of two in-phase and two anti-phase tilts along the *c*-axis which gives rise to a unit cell $\sqrt{2}a_{pc} \times \sqrt{2}a_{pc} \times 4a_{pc}$, where pc refers to the pseudo cubic lattice parameter, ≈3.92 Å.[20,22] The complex sequence of in-phase and anti-phase tilting quadruples the periodicity along *c* yielding ¼ order reflections along the *c*-axis in diffraction patterns. The differences between the three M phases involve subtle, non-symmetry breaking cation displacements that are described in detail elsewhere.[22,24] The B-site cations undergo local displacements that are strongly coupled to the oxygen octahedral rotations. Such a relationship is strongest at the M_2-M_3 phase transition at which point the local cations displacements undergo long-range ordering. In this temperature range a diffuse maximum in permittivity is observed making this region attractive for device applications.

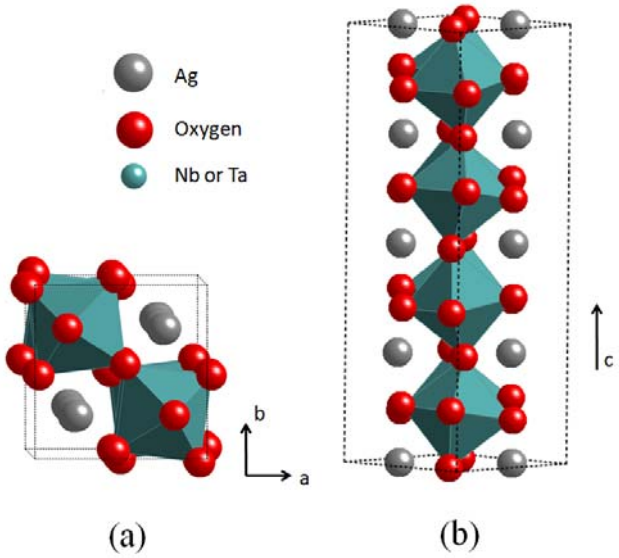

Figure 1 (Color online) M_3 structure of $AgNbO_3$ (a) viewed down the c-axis showing the combined in-phase and anti-phase tilting and (b) viewed along $<110>_o$ ($<100>_{pc}$) showing quadrupling of the unit cell along the c-direction

Recently, Han *et al.* reported that in relaxed $AgTa_{½}Nb_{½}O_3$ films on $LaAlO_3$ and $SrRuO_3/LaAlO_3$ substrates,[24] the M_3-M_2 phase transition was suppressed by ≈250 °C. It was proposed that the higher concentration of defects in the films disrupted the long-range ordering of local cation displacements. In contrast to the work reported by Han *et al*.,[24] this contribution focuses on coherently strained rather than relaxed films and aims to demonstrate the general principle that tilt transition temperatures may be modified using lattice strain. $AgTa_{½}Nb_{½}O_3$ films have therefore been grown on $SrTiO_3$ (a = 3.905 Å) substrates that have an in-plane lattice parameter smaller than that of $AgTa_{½}Nb_{½}O_3$ (≈3.92 Å), thereby inducing a compressive in-plane strain.

Experimental Procedure

Silver tantalate niobate thin films were prepared by chemical solution deposition using a process developed by Telli *et al*.[25] Niobium ethoxide and tantalum ethoxide were added to 2-methoxyethanol (2MOE). The solution was mixed at 110 °C after which a small volume was evaporated to remove any moisture. This solution was then mixed at 110 °C for 1 hour in a sealed flask in an argon atmosphere. In a separate container, silver nitrate was dissolved in pyridine and mixed at room temperature for one hour. The two solutions were then combined and mixed at 110 °C for 5 minutes. The molarity of the final solution was 0.1 M.

The solution was spun at 1500 rpm onto single crystal substrates of (001) $SrTiO_3$. After spinning, the film was subjected to two pyrolysis steps: one at 200 °C and one at 450 °C, both for 20 seconds. Films were then crystallized via rapid thermal annealing at 750 °C in oxygen for 1 minute with a heating rate of 100 °C/s. To prepare coherently strained films, only one layer was deposited to give a thickness of ≈15 nm. Two different compositions were studied: x=0 and x=0.5.

Structural characterization of the films was performed using X-ray diffraction and transmission electron microscopy (TEM). Lab source X-ray diffractometers (Scintag Pad V and Philips X'Pert Pro MRD 4-circle) were used to confirm phase purity and epitaxy. High resolution data were recorded on a Huber 4-circle diffractometer with a point detector at Sector 33-BM at the Advanced Photon Source using a photon energy of 21 keV. After heating the sample to ≈680 °C using an adjustable height furnace mounted to the diffractometer, data were collected every 25 °C on cooling. The reported thermal expansion of the substrate was used to calibrate the temperature.[26] Peak positions and integrated intensities were determined after fitting the peaks with Pseudo-Voigt and Gaussian functions.

Cross-sectional TEM foils were prepared by a standard procedure including mechanical polishing followed by Ar ion milling. Ion milling was carried out in a Fischione 1010 Ion Mill, operated initially at 3 kV and 5 mA and then at 0.5 kV and 3 mA once a perforation occurred. The specimens were cooled with liquid nitrogen throughout the ion milling process in order to minimize beam damage. High resolution imaging and electron diffraction were performed in a JEOL 2010f TEM, operated at 200 kV.

To distinguish between the crystallographic axes and the physical axes, *x* and *y* are used to describe the in-plane directions while *z* is used to describe the out-of-plane direction of the sample. Unless otherwise stated, all Miller indices and crystallographic axes will be given in the pseudo-cubic lattice.

Results and Discussion

Room Temperature Results

X-ray diffraction showed the films of both compositions to be phase-pure and epitaxial with the substrate. A reciprocal space map around the 113 Bragg peak (Figure 2) shows that the in-plane lattice parameters of $AgTa_{½}Nb_{½}O_3$ film are identical to the in-plane lattice parameters of the substrate, since *H* and *K* are the same for both peaks. For bulk ceramics, the room temperature lattice parameters are a = 5.5238 Å, b = 5.5673 Å, and c = 15.6721 Å.[27] Conversion to pseudocubic lattice parameters yields a_{pc} = 3.9059 Å, b_{pc} = 3.9366 Å, and c_{pc} = 3.918 Å. $SrTiO_3$ has a lattice parameter of 3.905 Å, which induces an in-plane compressive strain of ≈0.8% along the *b*-axis, ≈0.3% along the *c*-axis, and negligible strain along the *a*-axis. The strain state is similar at elevated temperatures.

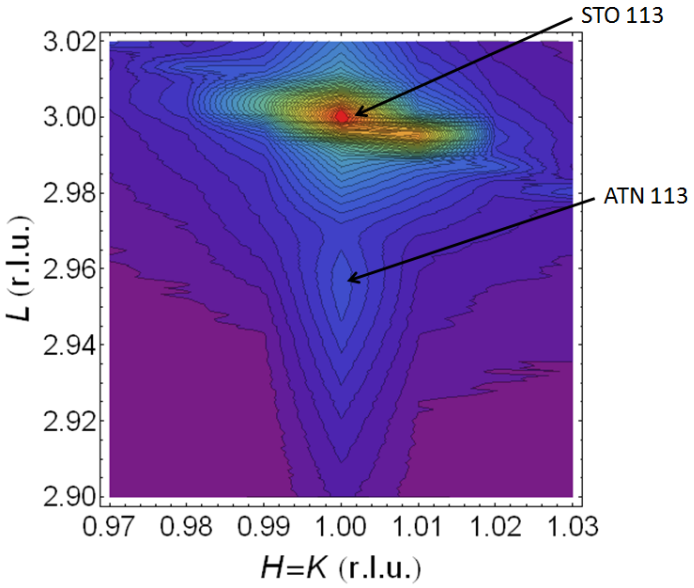

Figure 2 (Color online) Room temperature reciprocal space map around the 113 peak of a coherently strained $AgTa_{½}Nb_{½}O_3$ film on $SrTiO_3$. The film peak has the same *H* and *K* values as $SrTiO_3$, indicating that the film is coherently strained. The intensity is plotted on a log scale. Reciprocal lattice units (r.l.u.) are referenced to the room temperature lattice parameter of $SrTiO_3$.

Figure 3 shows a high resolution transmission electron micrograph (HRTEM) of the $AgTa_{½}Nb_{½}O_3$ film on $SrTiO_3$. The images show a clean interface between the film and substrate with no evidence for dislocations, porosity or Ag precipitates. The contrast at the interface is likely due to a combination of thickness variations and ion-milling artifacts.

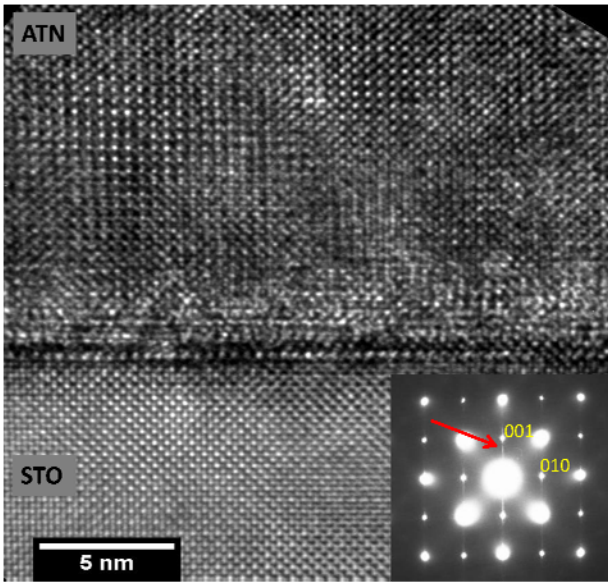

Figure 3 (Color online) High resolution transmission electron microscopic image of the $AgTa_{½}Nb_{½}O_3$ film on $SrTiO_3$ substrate. The image shows the film is homogeneous and free of secondary phases. Inset is an electron diffraction pattern obtained along the <100> zone axis. The pattern shows streaking along the *L*-direction (denoted by arrow) consistent with short range order of B-site cations.[22]

The room temperature phase of coherently strained films can be determined by examining ½{*ooo*} ± ¼{00*L*} reflections (*o* = odd index). At room temperature, bulk ATN exhibits the M-type structure with the tilt system $a^-b^-c^-/a^-b^-c^+$. The resulting quadrupling of the unit cell along the c_{pc} axis can be detected through quarter-order peaks that flank ½{*ooo*}-type reflections.[22] Figure 4 shows XRD profiles of *H*, *K*, and *L* scans in reciprocal space around the ½311 reflection at 25 °C. Reciprocal lattice units *H*, *K*, and *L* are given with respect to the $SrTiO_3$ substrate. Figure 4c shows finite intensity at the ¼-order positions suggesting that the films are in the M phase at room temperature. Peaks were not observed at the ½311 ± ¼00 and ½311 ± 0¼0 positions, indicating that the combined in-phase/anti-phase tilting occurs only along the out-of-plane direction. This differs from relaxed films in which the domain structure was such that the *c*-axis appeared in-plane as well as out-of-plane. The situation is counter-intuitive in the coherently strained films, given that the measured domain structure puts the long *b*-axis in the plane of the compressively strained film. From a strain perspective, the *b*-axis was likely to be the preferred out-of-plane axis.

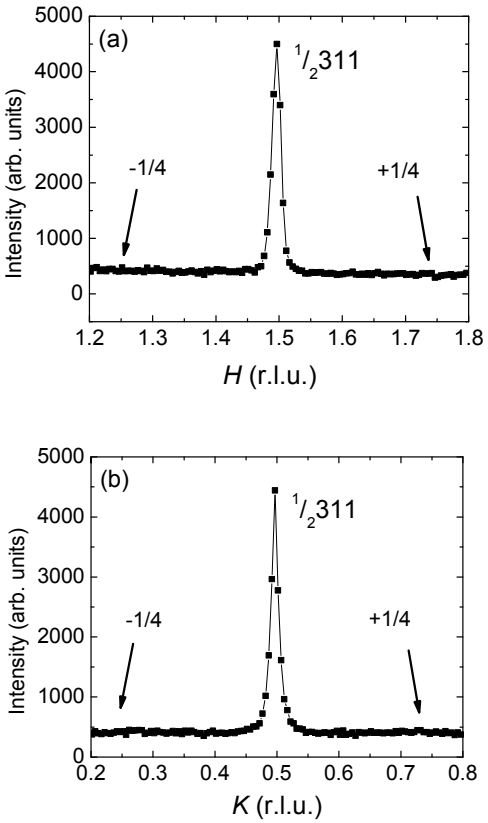

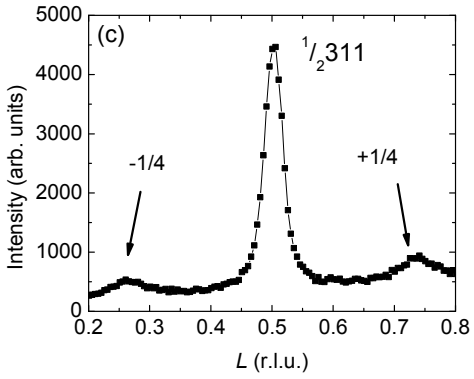

Figure 4 Intensity in reciprocal lattice units (r.l.u.) showing the (a) *H*, (b) *K*, and (c) *L* regions of reciprocal space around the ½311 peak for $AgTa_{½}Nb_{½}O_3$ films on $SrTiO_3$. The absence of intensity of ½311 ± ¼00 and ½311 ± 0¼0 indicate that the combined in-phase/anti-phase tilting occurs exclusively about the out-of-plane axis.

In addition to examining superlattice reflections due to octahedral tilting, superlattice reflections due to local cation displacements were also characterized to determine which M phase exists at room temperature in the $AgTa_{½}Nb_{½}O_3$ films. The M_3-M_2 phase transition marks the point at which local cation displacements undergo partial long-range ordering.[22] According to Levin *et al.*,[22] two consecutive B-site cations will displace along the [111] direction and the next two will displace along the $[11\bar{1}]$. The ordering of the B-site cations follows the periodicity imposed by the complex octahedral tilting about the *c*-axis and will also result in quarter-order superlattice reflections that flank the main Bragg peaks.

Figure **5** shows diffraction around the ATN 011 / $SrTiO_3$ 011 peaks. The difference in reciprocal lattice units, ΔL, is given with respect to the $SrTiO_3$ substrate. The absence of quarter order reflections indicates either that the long-range ordering of local cation displacements is disrupted in the coherently strained $AgTa_{½}Nb_{½}O_3$ films or that the peak intensity is below the detection threshold of the instrument. To assess which mechanisms dominate, compressively strained $AgNbO_3$ films were also examined. 011 ± 00¼ reflections (

Figure **5**b) were present, suggesting that there is considerably more local cation disorder in $AgTa_{½}Nb_{½}O_3$ films. Increased disorder of local cation displacements at room temperature is commensurate with the bulk ceramic phase diagram in which the M phase transition temperatures decrease as Ta concentration increases[20-22,27] and also with the observations on relaxed films by Han *et al*.[24]

For $AgTa_{½}Nb_{½}O_3$ films, no quarter order peaks appeared in either the *H* or *K* directions of reciprocal space. The background signal was significantly higher in the *L* direction compared to the *H* and *K* directions. This diffuse scattering can be attributed to truncation rods. The electron diffraction pattern from the <100> zone axis pattern (ZAP) is shown inset in Figure 3. Similar to XRD results, the *c*-direction shows streaks of diffuse intensity which can be interpreted as truncation rods. These results suggest that the coherent $AgTa_{½}Nb_{½}O_3$ films are in the M_3-like state with largely disordered local cation displacements at room temperature. Cryogenic measurements are required in order to determine the M_3-M_2 phase transition temperature in these films.

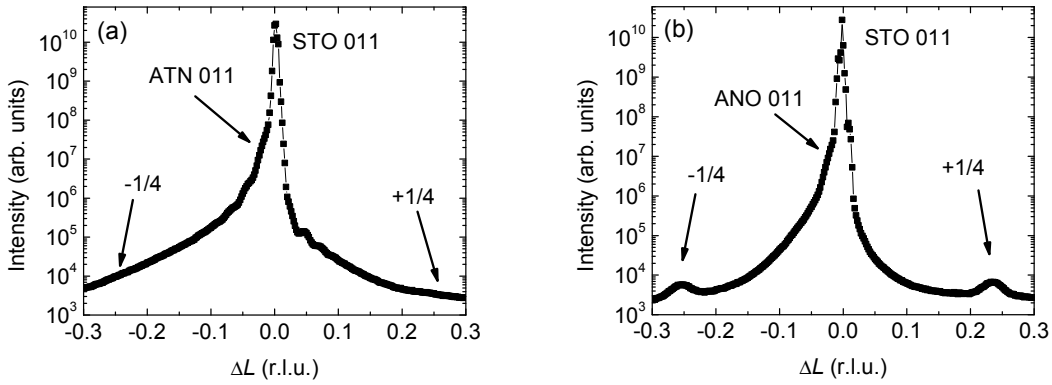

Figure 5 Diffraction from a room temperature *L*-scan in reciprocal space around the (a) 011 Bragg peak of $AgTa_{½}Nb_{½}O_3/SrTiO_3$ and (b) 011 Bragg peak of $AgNbO_3/SrTiO_3$. In (a) there is no evidence of quarter order reflections (arrows), suggesting that the B-site cations do not exhibit long range order in the ATN films. In (b), peaks are observed at – ¼ and +¼ positions. Δ*L* is given in reciprocal lattice units referenced to the $SrTiO_3$ substrate.

Phase Transitions

To assess the phase transition behavior of the coherently strained films, the lattice parameters were determined as a function of temperature. A Gaussian fit to the top of the film peak was used to determine the peak position. In Figure 6a, the difference in out-of-plane lattice parameters, $\Delta z = z_{ATN} - z_{STO}$, between $SrTiO_3$ and $AgTa_{½}Nb_{½}O_3$ is shown. The lattice parameter of $SrTiO_3$ increased linearly as a function of temperature; therefore, the anomalies at 200 °C and 400 °C in Figure 6a indicate phase transitions in the ATN film.

The anomalies in Figure 6a correspond to changes in the tilt system, as evidenced by changes to the superlattice reflections shown in Figure 6b. The T phase is tilted in-phase, which produces ½{*ooe*} superlattice reflections where *o* = odd and *e* = even indices.[28] Anti-phase tilting, which occurs in the M_3 phase about the *a*- and *b*-axes, results in ½{*ooo*} superlattice reflections. The O phase is ascribed to a mixed tilt system, reported as $a^0b^-c^+$, which produces anti-phase tilting about the *b*-axis and in-phase tilting about the *c*-axis. Figure 6b shows the normalized integrated intensity of ½311 (anti-phase tilting) and ½312 (in-phase tilting) peaks. Regions where the integrated intensity of ½311 dominate correspond to the M phase while regions where the integrated intensity of ½312 dominate correspond to the T phase. The O phase has finite intensity of both the in-phase and anti-phase superlattice reflections.

Transition temperatures between phases were determined by performing linear fits to the integrated intensity data in Figure 6b. The data was divided into intervals of 25 °C - 175 °C, 175 °C - 400°C and 400 °C - 650 °C. Each region was fitted with a straight line; the phase transition temperature was determined at the temperatures at which these lines intersected. Table 2 compares the transition temperatures of the compressively strained films to those of bulk $AgTa_{½}Nb_{½}O_3$. The data demonstrate that the M_3-O phase

transition in the films is suppressed by ≈150 °C, while the C-T transition temperature is increased by ≈130 °C. Thus, compressive biaxial strain expands the range of phase stability for the O and T phases.

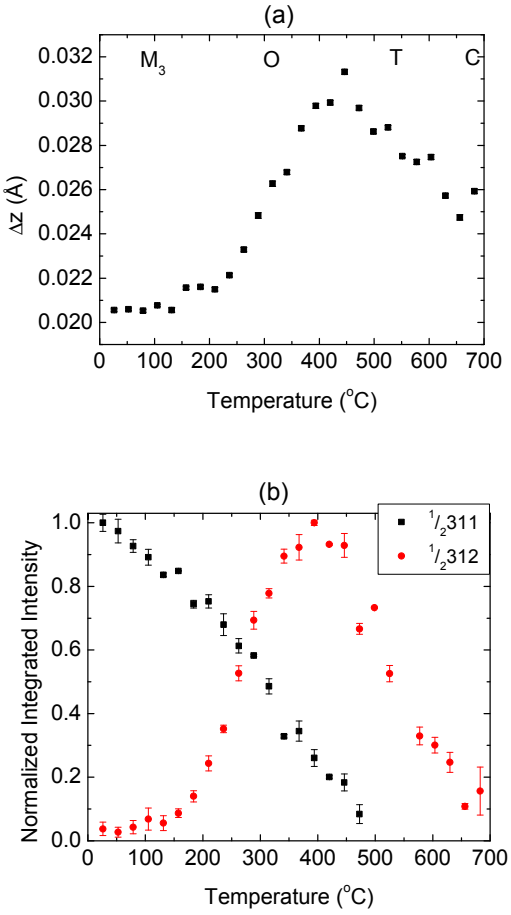

Figure 6 (Color online) (a) Δz of $AgTa_{½}Nb_{½}O_3$ films as a function of temperature. Because the lattice parameter of $SrTiO_3$ has a linear temperature dependence, anomalies in the data correspond to phase transitions in the ATN films. Error bars fall within the size of the data points. (b) Integrated intensity of ½311 and ½312 superlattice peaks normalized to the maximum intensity observed. In the M phase, anti-phase tilting dominates, whereas in the T phase, in-phase tilting dominates. The O phase has mixed in-phase and anti-phase tilting. This data show that the M-O phase transition occurs at 179 ± 12 °C, the O-T transition occurs at 378 ± 8 °C, and the T-C transition occurs at 682 ± 5 °C.

Table 2 Transition temperatures in compressively strained $AgTa_{½}Nb_{½}O_3$ films compared to bulk $AgTa_{½}Nb_{½}O_3$.

Transition Type	Bulk Transition Temperatures (°C)	Compressively Strained Films (°C)
C – T	552	682 ± 5
T – O	400	378 ± 8
O – M_3	326	179 ± 12

The M_3-O phase transition was confirmed by examining the integrated intensity of ½311 + 00¼ as a function of temperature, as shown in Figure 7. The quarter-order reflection disappears above 250 °C, 50 °C below the relaxed films described by Han *et al*.,[24] thereby confirming that the M_3-O transition has been suppressed due to strain in the film in agreement with data presented in Figure 6. The non-abrupt nature of the data at the phase transition suggests that either the tilt angle decreases or the coherence length for the tilt is reduced thereby making it difficult to ascertain the exact transition temperature with this data. This phenomenon can also be seen through the broadening of the full width at half maximum (FWHM) of the ½311 + 00¼ peak at temperatures near the phase transition (Figure 7b). At this point, it is not clear whether a decrease in the tilt angle or a reduction in coherence length is dominant in producing the divergence in the FWHM of the quarter-order peak. An estimate of the phase transition temperature can be determined by performing two linear fits to the FWHM data; one 25 – 175 °C and the second 175 – 275 °C. The phase transition temperature was found to be ≈ 180°C which agrees very well with that found in Table 2.

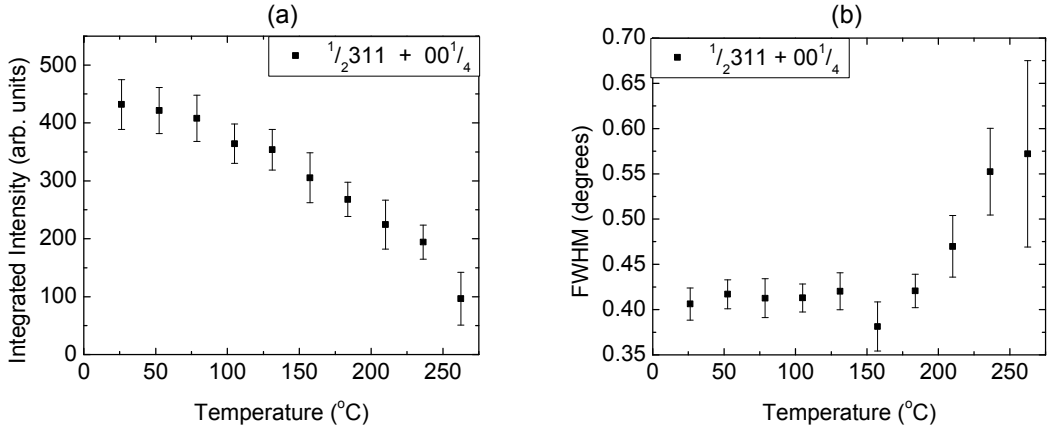

Figure 7 (a) Integrated intensity and (b) FWHM (phi scan) of the ½311 + 00¼ peak in $AgTa_{½}Nb_{½}O_3$ films. As temperature increases, the integrated intensity of the quarter order peak was not observed above 250 °C, indicating the film is in the O phase. The upward movement of the FWHM data suggests a transition temperature occurs ≈ 180 °C.

High Temperature Domain State

In order to determine the domain orientation in the tetragonal phase of these films, several ½{*ooe*} type reflections were recorded (*o* = odd, *e* = even). The tetragonal phase has a tilt system of $a^0a^0c^+$ with in-phase rotation around a single axis. Using rules for in-phase tilting developed by Glazer, the orientation of this unique axis may be determined. The Glazer rules are reproduced in Table 3 for convenience.[29] Figure 8 shows the intensities of the ½312, ½321 and ½123 peaks at 400 °C. Neither the ½321 or ½123 reflections showed measureable intensity, indicating that there are no rotations around the *y*-axis. It may be argued that for coherently strained films grown on a *P4mm* substrate, *x* and *y* are symmetrically equivalent. In this case, tilting about the *x*-axis should also be absent. In the figure, a well-developed ½312 is apparent. This suggests that the films exhibit in-phase tilt only along the out-of-plane *z*-axis.

Thus, the compressive in-plane strain has forced the film to adopt a domain structure in which the tilt rotation axis is out-of-plane, consistent with theoretical predictions and other experimental works.[4,9,10]

Table 3 List of superlattice reflections that are produced for in-phase tilt about the *x*-, y-, or z-axis. These rules are reproduced from Glazer.[29]

Tilt	Tilt Axis	Reflection
a^+	*x* or *y*	½{*eoo*} with *K*≠*L*
b^+	*x* or *y*	½{*oeo*} with *H*≠*L*
c^+	*z*	½{*ooe*} with *H*≠*K*

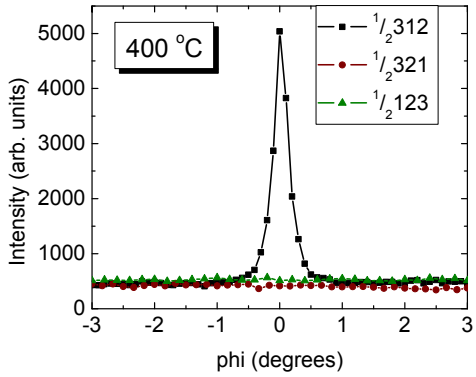

Figure 8 (Color online) The intensity of superlattice reflections of the type ½{*ooe*} for $AgTa_{½}Nb_{½}O_3$ films. The ½312 superlattice reflection is the only reflection that shows finite intensity in the tetragonal phase at 400 °C, suggesting that the in-phase tilt axis is out-of-plane and that domain states which would have put the tilt axis in-plane have been suppressed.

To date, there are no reports on the anisotropic properties of $AgTa_{½}Nb_{½}O_3$ due to the difficulty of producing untwinned crystals. The technique of domain control demonstrated here allows for the possibility to perform such a study on ATN.

Discussion

The schematic in Figure 9 illustrates domain evolution in compressively strained ATN films as a function of temperature. It is worth noting that in bulk ATN, the *a* and *b* lattice parameters in the T and O phases are smaller than the *c* lattice parameter. Conversely, in the M phases in bulk, the *b* lattice parameter of ATN is larger than both *a* and *c*. The films are crystallized at 750 °C when the material is in the cubic phase. As the sample cools from the cubic phase down into the T and O phases, the lattice mismatch is a minimum if the *c*-axis is out-of-plane. Therefore, the material preferentially adopts domain states in the T and O phases with the *c*-axis out-of-plane as was observed in Figure 8. As the coherently strained film is cooled into the M phases, the domains do not re-orient with the *c*-axis in the plane, even though this would minimize strain along this axis. Presumably, this is a result of the high activation energy associated

with reconfiguring the octahedral rotations. As a result, the complex tilt sequence develops normal to the substrate, and thus creates a domain state for M phase ATN in which the *c*-axis is exclusively along the out-of-plane direction.

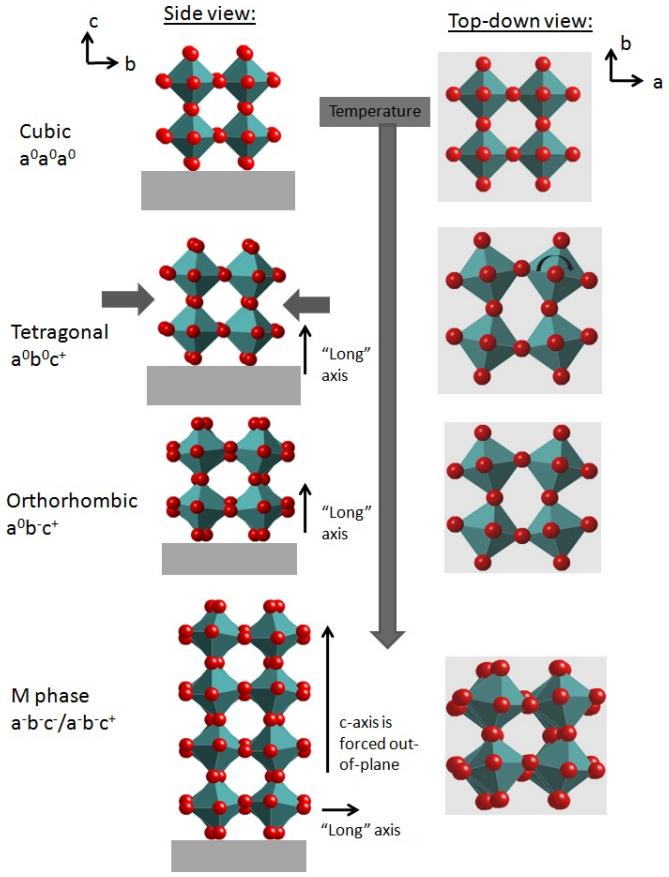

Figure 9 (Color online) In $AgTa_{½}Nb_{½}O_3$ films under compressive strain, the material is crystallized in the cubic phase. As it cools, the bi-axial in-plane strain forces the shorter *a*- and *b*- axes to lie in-plane while the *c*-axis (the "long" axis) pops out-of-plane. This configuration stabilizes the tetragonal and orthorhombic phases, resulting in these phase fields having an expanded temperature region compared to bulk. As the material cools further, the *c*-axis remains in the out-of-plane orientation even though the "long" axis is the *b*-axis.

Combining the information on tilt transition temperatures and that of local cation ordering, the phase transition temperatures of compressively strained $AgTa_{½}Nb_{½}O_3$ films can be superimposed on the bulk phase diagram, as shown in Figure 10. The phase transitions of the films, denoted by stars, show the expanded temperature region of the T and O phase fields. In addition, no indication of the M_2 phase was observed above room temperature. Although other compositions across the phase diagram were not studied, it is believed that the M3-O, O-T and T-C transitions would occur at comparable temperatures for various Ta/Nb concentrations. This results from the fact that the lattice parameter of ATN is a weak function of composition. Therefore, the strain state would be similar and the phase transition temperatures would be comparable across the phase diagram.

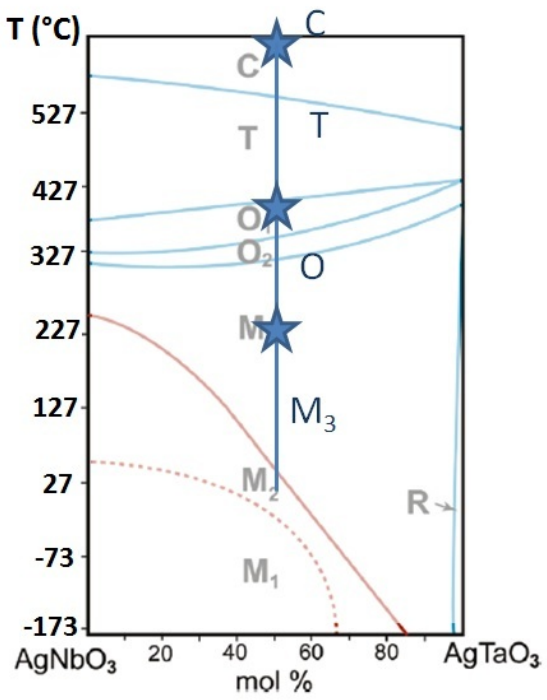

Figure 10 (Color online) Phase diagram for compressively strained $AgTa_{½}Nb_{½}O_3$ films on $SrTiO_3$ substrates superimposed on the bulk phase diagram for $AgTa_xNb_{1-x}O_3$ system. The stars indicate the phase transition temperatures observed in this work. The gray text represents the bulk phases while the black text refers to the films.

Conclusions

Coherent, compressively strained $AgTa_xNb_{1-x}O_3$ thin films were deposited on (001) $SrTiO_3$ substrates. The in-plane compressive biaxial strain expanded the temperature region of the O and T phase fields by ≈280 °C, and yielded a domain structure with the long axis out-of-plane. On further cooling, ferroelastic switching of the domain states was limited, which forced the complex tilt system to develop along the out-of-plane axis, despite the larger in-plane lattice mismatch. The strain control of the domain state in ATN films allows the possible study of anisotropy in such materials, as bulk materials and relaxed films are polydomain. As was the case for relaxed films, the coherently strained $AgTa_{½}Nb_{½}O_3$ films are in the M_3 phase at room temperature, while bulk ceramics and crystals are in the M_2 phase. This suggests that strain not only influences the octahedral rotations but also has an effect on the local cation displacements. This work demonstrates the first steps in strain engineering functional materials with complex tilt systems and compound phase transition sequences and opens up the possibility of tailoring functional properties that are influenced by octahedral rotations.

Acknowledgements

Financial support for this work is provided by the National Science Foundation (Materials World Network, DMR-0602770) and by the Engineering and Physical Science Research Council UK (EP/D067049/1G). Work at Argonne National Laboratory and the use of the Advanced Photon Source were supported by the U.S. Department of Energy, Office of Science, Office of Basic Energy Sciences, under Contract No. DE-AC02-06CH11357. Jenia Karapetrova's help at beamline 33-BM of the Advanced Photon Source, along with Pete Baldo's technical assistance is gratefully acknowledged.

References

(1) Eitel, R.; Randall, C. A. *Physical Review B* **2007**, *75*, 094106.

(2) Reaney, I. M.; Colla, E. L.; Setter, N. *Japanese Journal of Applied Physics Part 1-Regular Papers Short Notes & Review Papers* **1994**, *33*, 3984.

(3) Tinberg, D. S.; Johnson-Wilke, R. L.; Fong, D. D.; Fister, T. T.; Streiffer, S. K.; Han, Y. S.; Reaney, I. M.; Trolier-McKinstry, S. *Journal of Applied Physics* **2011**, *109*.

(4) Hatt, A. J., Spaldin, N.A. In *arXiv:0808.3792v1* 2008.

(5) Rondinelli, J. M.; Coh, S. *Physical Review Letters* **2011**, *106*.

(6) Rondinelli, J. M.; Spaldin, N. A. *Physical Review B* **2010**, *82*.

(7) He, F. Z.; Wells, B. O.; Ban, Z. G.; Alpay, S. P.; Grenier, S.; Shapiro, S. M.; Si, W. D.; Clark, A.; Xi, X. X. *Physical Review B* **2004**, *70*, 235405.

(8) He, F. Z.; Wells, B. O.; Shapiro, S. M. *Physical Review Letters* **2005**, *94*, 176101.

(9) May, S. J.; Kim, J. W.; Rondinelli, J. M.; Karapetrova, E.; Spaldin, N. A.; Bhattacharya, A.; Ryan, P. J. *Physical Review B* **2010**, *82*, 014110.

(10) Vailionis, A.; Boschker, H.; Siemons, W.; Houwman, E. P.; Blank, D. H. A.; Rijnders, G.; Koster, G. *Physical Review B* **2011**, *83*.

(11) May, S. J.; Smith, C. R.; Kim, J.-W.; Karapetrova, E.; Bhattacharya, A.; Ryan, P. J. *Physical Review B* **2011**, *83*, 153411.

(12) Choi, K. J.; Baek, S. H.; Jang, H. W.; Belenky, L. J.; Lyubchenko, M.; Eom, C. B. *Advanced Materials* **2010**, *22*, 759.

(13) Vailionis, A.; Siemons, W.; Koster, G. *Applied Physics Letters* **2007**, *91*.

(14) Vailionis, A.; Siemons, W.; Koster, G. *Applied Physics Letters* **2008**, *93*.

(15) Valant, M.; Suvorov, D. *Journal of the American Ceramic Society* **1999**, *82*, 81.

(16) Valant, M.; Axelsson, A. K.; Alford, N. *Journal of the European Ceramic Society* **2007**, *27*, 2549.

(17) Petzelt, J.; Kamba, S.; Buixaderas, E.; Bovtun, V.; Zikmund, Z.; Kania, A.; Koukal, V.; Pokorny, J.; Polivka, J.; Pashkov, V.; Komandin, G.; Volkov, A. *Ferroelectrics* **1999**, *223*, 235.

(18) Kim, H. T.; Shrout, T.; Randall, C.; Lanagan, M. *Journal of the American Ceramic Society* **2002**, *85*, 2738.

(19) Grinberg, I.; Rappe, A. M. *Applied Physics Letters* **2004**, *85*, 1760.

(20) Sciau, P.; Kania, A.; Dkhil, B.; Suard, E.; Ratuszna, A. *Journal of Physics-Condensed Matter* **2004**, *16*, 2795.

(21) Kania, A. *Phase Transitions* **1983**, *3*, 131.

(22) Levin, I.; Krayzman, V.; Woicik, J. C.; Karapetrova, J.; Proffen, T.; Tucker, M. G.; Reaney, I. M. *Physical Review B* **2009**, *79*, 104113.

(23) Glazer, A. M. *Acta Crystallographica Section B-Structural Science* **1972**, *B 28*, 3384.

(24) Han, Y.; Reaney, I. M.; Johnson-Wilke, R. L.; Telli, M. B.; Tinberg, D. S.; Levin, I.; Fong, D. D.; Fister, T. T.; Streiffer, S. K.; Trolier-McKinstry, S. *Journal of Applied Physics* **2010**, *107*, 123517.

(25) Telli, M. B.; Bharadwaja, S. S. N.; Biegalski, M. D.; Cheng, J. G.; Trolier-McKinstry, S. *Journal of Applied Physics* **2007**, *101*.

(26) Touloukain, Y. S. In *Thermophysical Properties of Matter* IFI/Plenum: 1977; Vol. 13.

(27) Levin, I.; Woicik, J. C.; Llobet, A.; Tucker, M. G.; Krayzman, V.; Pokorny, J.; Reaney, I. M. *Chemistry of Materials* **2010**, *22*, 4987.

(28) Woodward, D. I.; Reaney, I. M. *Acta Crystallographica Section B-Structural Science* **2005**, *61*, 387.

(29) Glazer, A. M. *Acta Crystallographica Section A* **1975**, *31*, 756.